Efficient Convolutional Neural Network for Brain Tumor Classification from MRI Scans

CS679 - Final Project Report

Sky Qiao, Shujie Liu, Joseph Zou, Ali Raisolsadat

Abstract

In this study, we propose a novel Convolutional Neural Network architecture for a four-class classification task on brain tumors MRI scans. We evaluated the performance of our proposed model against state-of-the-art pre-trained models using average class accuracy and computational cost. Our findings show that our model serves as a valuable alternative, achieving comparable accuracy to leading pre-trained models while significantly reducing computational cost.

Introduction.

Brain Tumors.

Brain tumors are a serious health concern in North America, affecting thousands yearly. In the United States, approximately 88970 new cases of primary brain tumors were diagnosed in 2022, with a 5-year relative survival rate for those with malignant brain or nervous system tumors of only 36%. The prognosis for brain tumors is often poor, as brain and other nervous system tumors account for approximately 18200 people's deaths as a result of a primary malignant brain tumor in 2022. There are currently more than 28000 children in the United States are currently diagnosed with brain tumors [1]. In Canada, brain cancer is also a significant health concern. An estimated 3200 people were diagnosed with the disease in 2022, with a 5-year relative survival rate for those with malignant brain or nervous system tumors of only 21% [2]. These statistics demonstrate brain tumors' impact on individuals and families and the importance of supporting research and treatment efforts to improve outcomes for those affected. Brain tumors can disrupt the brain's regular operations, which govern all bodily functions. They may increase in size and press against critical structures within the brain. There are three families of tumors dominant in adults, namely Glioma, Meningioma, and Pituitary tumors.

The symptoms of gliomas may include aphasia (problems with speaking and communicating), changes in vision or vision loss, and cognitive problems. The common signs and symptoms of pituitary tumors include headaches, nausea, vomiting, confusion, or a decline in brain function, such as problems with thinking and understanding information, memory loss, personality changes or irritability, and vision problems. Furthermore, meningioma symptoms depend on where in the brain or, rarely, the spine the tumor is situated; signs and symptoms may include vision changes, such as seeing double or blurriness, headaches, hearing loss, memory loss, loss of smell, seizures, weakness in the arms or legs that worsens over time. In addition, depending on the tumor's size and position, it may lead to life-threatening complications such as brain swelling, bleeding, or blockage of cerebrospinal fluid flow [3][4]. Brain tumors can appear in anyone, regardless of age, gender, or race. However, some brain

tumor types are more frequent in specific age groups. For instance, meningiomas are more prevalent in older adults, while medulloblastomas are more common in children [5][6]. These tumors may have various causes, most of which are unknown. Exposure to radiation, genetic syndromes, and weakened immune systems are among the identified risk factors. Nevertheless, in many cases, the origin of a brain tumor remains unidentified. Primary brain tumors, which arise within the brain, are relatively uncommon, accounting for just 1% of all cancers [7][8].

MRI Scans.

Due to the severity of brain tumors (and other types of cancers), the medical imaging technology, such as computed axial tomography scans (CT scans) and magnetic resonance imaging (MRI), underwent a significant revolution in the 20th century, enabling medical professionals to diagnose brain tumors more accurately [9]. Magnetic Resonance Imaging (MRI) is a medical imaging technique that uses a strong magnetic field and radio waves to generate detailed images of the body's internal structures. These machines can diagnose various medical conditions, including brain and spinal cord injuries, tumors, and abnormalities in the joints and soft tissues. An MRI machine has a large, circular magnet that produces a strong, uniform magnetic field. When a patient enters the machine, the magnetic field causes the protons in their body to align with the magnetic field. The machine then emits radio waves, which cause the protons to absorb and release energy. A receiver coil detects the energy released by the protons, and the information from the energy released generates detailed images of the body's internal structures [10]. MRI is an essential tool in modern medicine, and ongoing research is underway to improve the technology and expand its applications.

However, an MRI machine alone cannot diagnose and requires a practitioner (doctor or radiologist) to make a precise diagnosis. Therefore, due to the reliance on doctors' expertise, there is still room for human error in the diagnosis process. Inexperienced doctors may make incorrect diagnoses, resulting in missed opportunities for optimal treatment. Even experienced doctors may occasionally make mistakes or exhibit biased diagnoses based on their exposure to various brain tumors throughout their careers.

CNN.

Artificial neural network(ANN) is a machine learning method which is inspired by the structure and function of human brains. In particular, an ANN usually consists of multiple interconnected layers, and each layer contains neurons which process input signals and pass them onto the next layers. Given input data, the neural network can learn to capture the dynamics of the data by changing the strength of connection between the neurons. ANNs have been proven effective and have brought about revolutionary advances across numerous fields, such as image classification and natural language processing. Convolutional Neural Network(CNNs) is a type of ANN model which contains convolutional layers on top of regular fully connected layers. Such architecture allows the neural network to capture input data's spatial correlations, making it highly effective for the image classification task. In some cases, such as characterizing the composition of bioleaching bacterial biofilms, neural networks can even outperform human experts in image classification [11].

CNNs have become a popular approach for detecting brain tumors in MRI scans because they can automatically extract relevant features from the images. With CNNs, there is no need for manual feature engineering as they can extract the shape and texture features of the tumor from the scans. Additionally, CNNs can leverage large datasets for learning, allowing them to identify more complex relationships between features and the presence of tumors. CNNs also have a non-linear mapping

function, making it possible to capture intricate relationships between features and tumor presence. Furthermore, CNNs are designed to be robust to noise and artifacts commonly found in MRI scans, enabling them to learn to ignore irrelevant features. Finally, once trained, CNNs can quickly and efficiently analyze new MRI scans, reducing the time it takes to diagnose and treat patients [12].

This project is inspired by and built upon the work of Sharma et al., which uses CNNs on heart MRI scans to classify heart disease [13]. We adopted a similar approach by integrating CNNs with brain tumor MRI scans. This study aims to develop a model that can accurately classify patients into four classes - glioma, pituitary, meningioma, and no tumor - based on their MRI scans. We found that naively applying the architecture proposed by Sharma et al. on our brain tumor images dataset is not highly effective. Hence, we proposed a different CNN architecture that allows us to better capture the complexity of the brain tumor images. Notably, our proposed model achieves comparable accuracy with the state-of-the-art model, but our model is significantly more efficient in terms of computational cost. Our result could help speed up the diagnosis process, assisting radiologists with early diagnosis of brain tumors and aiding neurologists in classifying tumor types. It can also help differentiate regrowing tumors from scar tissue in post-surgery MRI scans, a common source of misdiagnosis for doctors.

Introduction to Data.

We gathered 3264 MRI scans of brains captured in three cross-sectional positions: axial, coronal, and sagittal (Figure 1) [14]. These scans are grouped into four classes: glioma tumors, pituitary tumors, meningioma tumors, and no tumors. The three tumor classes' datasets have relatively balanced sizes(926, 901, and 937, respectively), and the "no tumor" class's dataset has a smaller size with 500 images. We randomly split our dataset into training and test sets for each of themodels discussed in the following sections.

The dataset for this project includes a mix of both T1 and T2 weighted, in different cross-sectional planes. T1 and T2 weighted images are two MRI types commonly used in clinical practice. T1-weighted images have a short repetition time (TR) and a short echo time (TE), which leads to a high signal intensity from tissues with short relaxation times, such as fat and gadolinium contrast agents. In contrast, tissues with longer relaxation times, such as muscle and gray matter, have lower signal intensity on T1-weighted images. Therefore, T1-weighted images of the brain present bone and air as black, while bone marrow and other soft tissues are gray or white. T2-weighted images have a long TR and a long TE, which leads to high signal intensity from tissues with long relaxation times, such as fluid and edema. In contrast, tissues with shorter relaxation times, such as bone and cortical gray matter, have lower signal intensity on T2-weighted images. Hence, T2-weighted images of the brain present bone and air as high contrast (white or light gray), while bone marrow and other soft tissues are dark gray or black. The axial, coronal, and sagittal planes are the three standard anatomical planes (cross-sectional positions) used to view MRI images. The axial plane is oriented perpendicular to the body's long axis and runs horizontally from front to back. The coronal plane is oriented perpendicular to the sagittal plane and runs vertically from side to side, dividing the body into front and back sections. The sagittal plane is oriented perpendicular to the axial and coronal planes and runs vertically from front to back, dividing the body into left and right sections [15].

From our dataset, it is evident that there is a class imbalance issue with the "no tumor" class in MRI tumor classification studies. This imbalance is because patients seek medical attention when they experience symptoms or suspect that they may have a medical condition, such as a brain tumor. In contrast, patients with no symptoms or concerns about their health may not seek medical attention

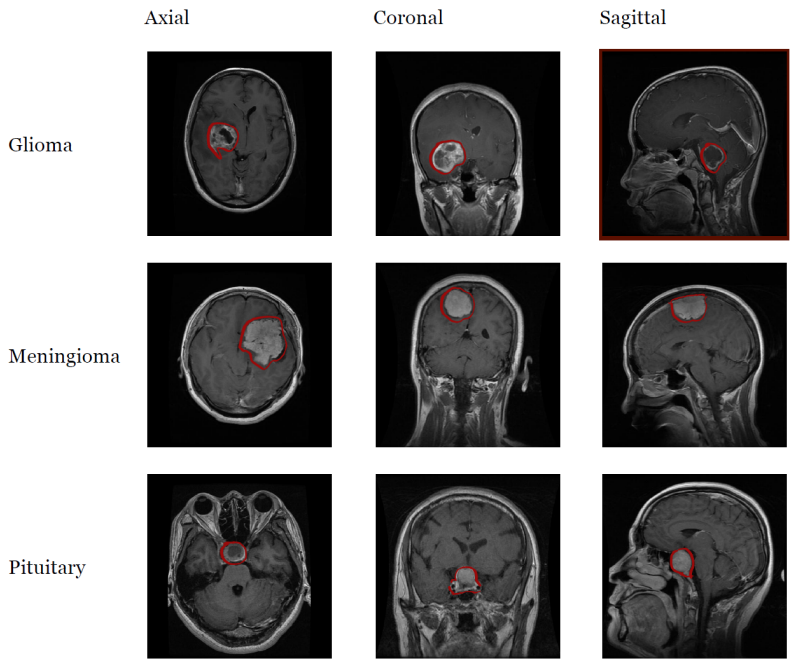

Fig. 1: T1-weighted MRIs of 3 types of brain tumors, 1. Glioma, 2. Meningioma, and 3. Pituitary. Images are in 3 cross-sectional positions of 1. axial, 2. coronal, and 3. sagittal.

and thus may not be included in the dataset. As a result, the "no tumor" class may have fewer cases available for training this project's model. We believe that this is a realistic representation of the class imbalance we would obtain in real life applications. However, there are potential issues with class imbalance. For example, it can lead to (1) biased model, where the model can achieve high accuracy by simply predicting the majority class for every input, leading to poor performance for the minority class and the model not learning to differentiate between the classes effectively [16], (2) poor generalization, by causing the model to overfit on the majority class and perform poorly on new and unseen data [17], and (3) decrease in interpretability, where the model learns to rely on the dominant features in the majority class and ignore the essential features of the minority class, making it challenging to interpret the model's decision-making process [18].

Furthermore, in practice, the data labels are generated following a comprehensive clinical evaluation of the patient's symptoms and differential diagnosis. This clinical evaluation includes extensive analysis by neurosurgeons and radiologists of the MRI and CT scans and invasive procedures such as neuro endoscopy (less invasive) or brain biopsy (very invasive). Some labels may also be produced during the postmortem examination of the patient. In the context of this project, the dataset has been cleaned through manual examination of the MRI scans by the uploading team. Additionally, a specialist was consulted to examine all the MRIs, as evidenced by the certification provided by the physician, which can be found in *appendix A.1*.

Methodology.

In this section, we will discuss the different CNN architectures experimented in the project, and motivation for considering them.

Model Proposed for Detecting Heart Disease from MRI Scans.

As the work of Sharma et al. inspires our project for classifying heart disease from MRI scans, we started with implementing and experimenting with their proposed CNN architecture. In particular, this architecture is a standard CNN model with two convolutional layers with kernel size (5×5) and padding/stride size of 1, two max-pooling layers of size (2×2), and two fully connected layers with ReLU and Sigmoid activation (Figure 2). It takes greyscale inputs of size $(28 \times 28 \times 1)$ and produces predicted labels for detecting global hypokinesia. We modified the last fully connected layer to adopt this architecture on the brain tumor dataset to have four nodes for our four-class classification task. We changed the activation and loss functions to Softmax activation and Cross Entropy loss.

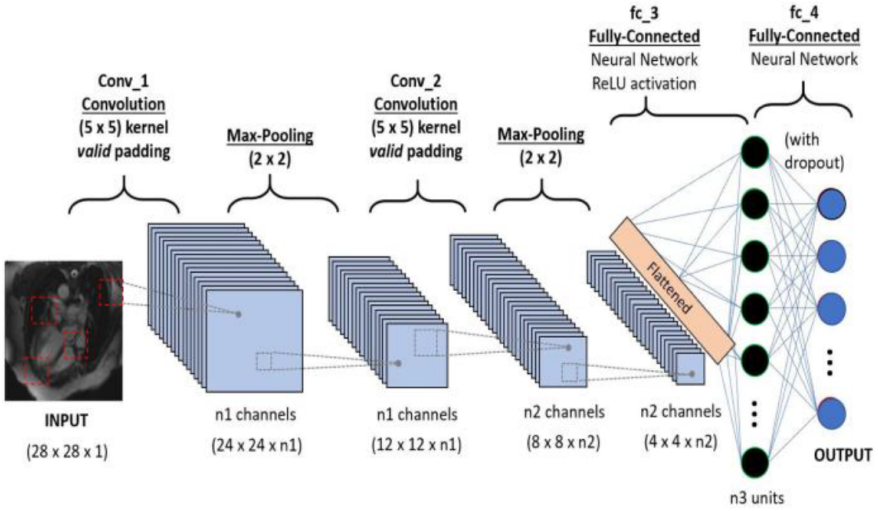

Fig. 2: Model proposed by Sharma et al. "Classification of Heart Disease from MRI Images Using Convolutional Neural Network.

Proposed Architecture.

Since MRI scans usually come with high resolution, resizing them to the size of (28×28) may lead to the loss of important information in the images that can potentially be useful in classifying them. Hence, we propose to use a deeper CNN that can handle higher-resolution pictures. In particular, we kept the convolutional layer's kernel size at (5×5), the padding/stride size at 1, and the pooling layer's kernel size at (2×2). We experimented with other architecture choices summarized in Table 1. Among these choices, the architecture that takes an input size of $(124 \times 124 \times 3)$ with four convolutional layers and four Max-Pooling layers performs best. Figure 3 shows our final model. We added a batch normalization layer and a ReLU activation layer after each convolutional layer for faster convergence and better performance. We also added a 50% dropout layer in the fully connected layers to avoid overfitting, and we used gradient clipping to handle the gradients exploding/vanishing problem.

Transfer Learning.

Transfer learning [19] is a popular technique for image classification tasks. It relies on pre-trained models, where the weights are pre-trained on a large dataset such as ImageNet, which contains more than 14 million samples. These pre-trained models are then fine-tuned by updating the weights of

	Choices
Input Size	124*124*3, 252*252*3, 508*508*3
# of Conv Layers	4, 5, 6
# of Pooling Layers	4, 5, 6
Pooling Method	Max Pooling, Mean Pooling

Tab. 1: Summary of architecture choices.

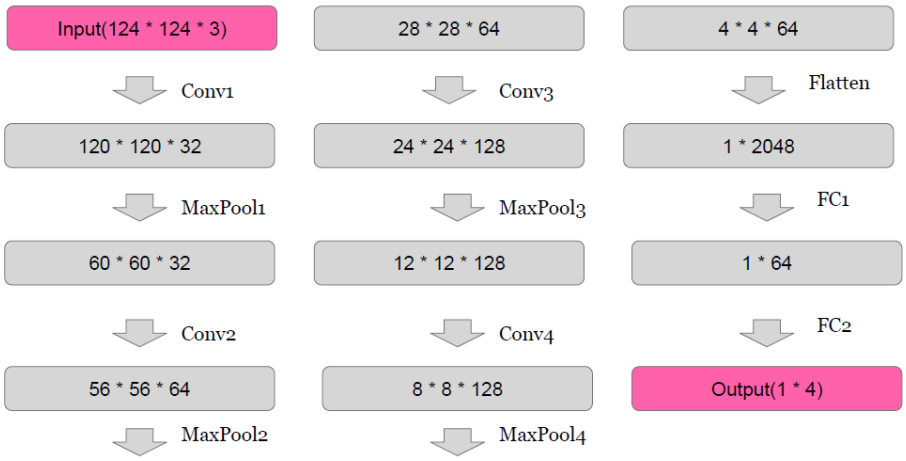

Fig. 3: Proposed architecture.

several or all layers to suit the specific task. In our study, we utilize this technique on the following models, using them as a benchmark to evaluate the performance of our proposed architecture.

State-of-the-Art Architecture.

We also consider state-of-the-art architectures for medical imaging classification problems. The first model we considered is ResNet-50 [20]. This architecture has 50 layers and utilizes the skip connections, allowing it to be very deep without suffering from the gradient vanishing/exploding problems. The second model we considered is VGG-16 [21]. This architecture uses small filters of size (3×3), allowing it to learn complex features with fewer parameters. The third model we considered is EfficientNet [22]. This architecture aims to maintain a balance over the number of parameters, number of layers, and image sizes to achieve better performance and efficiency.

U-Net.

U-Net [23] was originally developed for image segmentation tasks. Here, we use a pre-trained U-Net as a first-step feature extraction tool, and we add convolutional layers and a classifier to it for further feature extraction and classification.

Vision Transformer.

Vision Transformer [24] was first introduced in the context of Natural Language Processing, and in recent years, researchers have successfully applied it to Computer Vision. In particular, the Vision

Transformer is an image classification model, and in our study, we consider the pre-trained ViT-B/16 model.

For all the aforementioned models, to handle the class imbalance issue, we experimented with assigning more weights to the minority class of "no tumor" in the loss function. Having weighted loss can potentially help the model to generalize better as it avoids over/underrepresentation for the classes. We also used a more accurate evaluation for model accuracy by using the average class accuracy instead of the overall accuracy. In particular, the accuracy is calculated as:

$$\text{Class Accuracy} = \frac{\text{\# of correctly classified instances in a class}}{\text{\# instances in a class}} \times 100\% \tag{0.0.1}$$

$$\text{Accuracy} = \text{Mean(Class Accuracy)} \tag{0.0.2}$$

We used the Adam optimizer for all the models. We also experimented with different hyperparameters choices for each of the models. These choices are summarized in Table 2. For each model mentioned above, the best choices are selected using cross-validation and summarized in Table 3.

	Choices
Class Weights	(1,1,1,1), (1,1,2,1)
Weight Decay	1e-1, 1e-2, 1e-3, 1e-4, 1e-5, 0
Learning Rate	1e-1, 1e-2, 1e-3, 1e-4, 1e-5

Tab. 2: Summary of class weights and hyperparameter choices.

	Heart disease paper	Proposed architecture	ResNet-50	VGG-16	EfficientNet	U-Net	ViT-B/16
Class Weights	(1,1,2,1)	(1,1,1,1)	(1,1,1,1)	(1,1,1,1)	(1,1,2,1)	(1,1,1,1)	(1,1,1,1)
Weight Decay	0	1e-5	0	1e-3	1e-5	0	0
Learning Rate	1e-3	1e-4	1e-4	1e-5	1e-4	1e-4	1e-4

Tab. 3: Summary of selected class weights and hyperparameters for each model.

Model Results and Analysis.

We evaluated the performance of the models described above using a 9:1 training/test split and summarized the results in Table 4. We compared our proposed model with the other models using two metrics: (1) average class accuracy on the test set; and (2) total run time (i.e. training and testing time combined) on a GeForce 3060Ti GPU. Our proposed model achieved average class accuracy of 97.03% when trained from scratch, which is close to the accuracy achieved by the pre-trained models of 97.86%-99.15%. In addition, our model outperformed the model by Sharma et al, which achieved an accuracy of 90.84%. Regarding computational efficiency, our proposed model was significantly more efficient than the others with comparable accuracy. In particular, it is around 3.6x faster than EfficientNet and ResNet-50, and more than 10x faster than VGG-16, U-Net and ViT-B/16.

Since it is often hard to collect medical images due to cost and privacy concerns, we also want to evaluate our model's performance in the context of few-shot learning, which involves training a model

	Heart Disease Paper	Proposed Architecture	ResNet-50	VGG-16	EfficientNet	U-Net	ViT-B/16
Average Class Accuracy	90.84%	97.03%	99.15%	98.37%	99.19%	88.12%	97.86%
Total Runtime	165s	351s	1311s	5052s	1218s	4111s	4567s

Tab. 4: Comparison of model performance based on average class accuracy and runtime using 9:1 training/test split.

with an extremely small dataset (usually 1-10 samples per class). We compare our model's performance with the other models under the 1:9 and 1:99 training/test split. With a 1:9 training/test splits, each class has around 90 samples in the training set (the "no tumor" class has around 50 samples in the training set); with a 1:99 training/test split, each class has around 9 samples in the training set ("no tumor" class has around 5 samples in the training set). Table 5 gives a summary of the results. We see that in terms of accuracy, the pre-trained models had the best performance, and our model can only beat some pre-trained models when the training/test split is 1:99. Regarding computational efficiency, our model largely beats all the pre-trained models. Therefore, when the training set is large, our proposed model can achieve close to state-of-the-art pre-trained models' accuracy at half the computational cost. When the training set is small, our proposed model can also be an excellent candidate as it gives comparable accuracy to some state-of-the-art models at much less computational cost.

	Heart Disease Paper	Proposed Architecture	ResNet-50	VGG-16	EfficientNet	U-Net	ViT-B/16
Average Class Accuracy	70.74%	76.56%	89.27%	83.46%	87.70%	57.35%	84.98%
Total Runtime	38s	59s	205s	479s	169s	641s	660s
Average Class Accuracy	49.55%	54.76%	54.56%	62.28%	58.61%	32.35%	49.63%
Total Runtime	13s	24s	77s	146s	63s	221s	222s

Tab. 5: Comparison of model performance based on average class accuracy and runtime using 1:9 training/test split and 1:99 training/test split.

Concluding Remarks and Future Work.

In conclusion, we proposed an efficient CNN architecture that achieves comparable accuracy to leading pre-trained models on brain tumor MRI scans, while costing 3-10x less computational power, and outperforming some state-of-the-art models when limited training data is provided. Our work can be valuable in reducing human error in manual brain tumor diagnosis by doctors, speeding up the diagnosis process, and improving patient care through early diagnosis and treatment. Note that an area for future improvement is to develop an architecture that can achieve/beat pre-trained models' accuracy in few-shot learning scenarios at a lower computational cost. Future work may also focus on utilizing this brain tumor MRI dataset for image segmentation purposes. For example, the previously described U-Net architecture can be used to generate a pixel-wise classification of the MRI scans. This method can potentially help doctors/radiologists locate the tumor more accurately and speed up the diagnosis process even further.

References

[1] Cronin, KA, Scott, S, Firth, AU, et al. Annual report to the nation on the status of cancer, part 1: National cancer statistics. *Cancer. 2022; 128*(24): 4251- 4284. doi:10.1002/cncr.34479

[2] Darren R. Brenner, Abbey Poirier, Ryan R. Woods, Larry F. Ellison, Jean-Michel Billette, Alain A. Demers, Shary Xinyu Zhang, Chunhe Yao, Christian Finley, Natalie Fitzgerald, Nathalie Saint-Jacques, Lorraine Shack, Donna Turner, Elizabeth Holmes. *Projected estimates of cancer in Canada in 2022*. May 2022, 194 (17) E601-E607; DOI: 10.1503/cmaj.212097

[3] Brain tumor - Diagnosis and treatment - Mayo Clinic. (2023, February 10). Retrieved March 8, 2023, from https://www.mayoclinic.org/diseases-conditions/brain-tumor/diagnosis-treatment/drc-20350088

[4] Niederhuber JE, et al., eds. Cancer of the central nervous system. *Abeloff's Clinical Oncology. 6th ed*. Elsevier; 2020. Accessed March. 1, 2023.

[5] Louis, D. N., Perry, A., Wesseling, P., Brat, D. J., Cree, I. A., Figarella-Branger, D., Hawkins, C., Ng, H. K., Pfister, S. M., Reifenberger, G., Soffietti, R., Von Deimling, A., & Ellison, D. W. (2021). The 2021 WHO Classification of Tumors of the Central Nervous System: a summary. *Neuro-Oncology, 23*(8), 1231–1251. https://doi.org/10.1093/neuonc/noab106

[6] Kliegman, R. M., & St. Geme, J. S. (2019). *Nelson Textbook of Pediatrics E-Book*. Elsevier Gezondheidszorg.

[7] Bondy, M. L., Houlston, R. S., Malmer, B., Barnholtz-Sloan, J. S., Davis, F. G., Il'yasova, D., Kruchko, C., McCarthy, B. J., Rajaraman, P., Schwartzbaum, J. A., Sadetzki, S., Schlehofer, B., Tihan, T., Wiemels, J. L., Wrensch, M., & Buffler, P. A. (2008). *Brain tumor epidemiology: Consensus from the Brain Tumor Epidemiology Consortium. Cancer, 113*(S7), 1953–1968. https://doi.org/10.1002/cncr.23741

[8] De Robles, P., Fiest, K. M., Frolkis, A. D., Pringsheim, T., Atta, C., St Germaine-Smith, C., Day, L., Lam, D., & Jette, N. (2015). The worldwide incidence and prevalence of primary brain tumors: a systematic review and meta-analysis. Neuro-Oncology, 17(6), 776–783. https://doi.org/10.1093/neuonc/nou283

[9] Lauterbur, P. C. (1973). Image Formation by Induced Local Interactions: Examples Employing Nuclear Magnetic Resonance. *Nature, 242*(5394), 190–191. https://doi.org/10.1038/242190a0

[10] McRobbie, D., Moore, E., Graves, M., & Prince, M. (2006). *MRI from Picture to Proton (2nd ed.)*. Cambridge: Cambridge University Press. doi:10.1017/CBO9780511545405

[11] Buetti-Dinh, A., Galli, V., Bellenberg, S., Ilie, O., Herold, M., Christel, S., Boretska, M., Pivkin, I. V., Wilmes, P., Sand, W., Vera, M.,& Dopson, M. (2019). Deep neural networks outperform human expert's capacity in characterizing bioleaching bacterial biofilm composition. *Biotechnology Reports, 22, e00321*. https://doi.org/10.1016/j.btre.2019.e00321

[12] Kim M, Yun J, Cho Y, Shin K, Jang R, Bae HJ, Kim N. Deep Learning in Medical Imaging. *Neurospine*. 2019 Dec;16(4):657-668. https://doi.org/10.14245/ns.1938396.198

[13] Sharma, A. K., Kumar, R., & Jaiswal, V. (2021b). Classification of Heart Disease from MRI Images Using Convolutional Neural Network. *International Conference on Signal Processing*. https://doi.org/10.1109/ispcc53510.2021.9609408

[14] Sartaj Bhuvaji, Ankita Kadam, Prajakta Bhumkar, Sameer Dedge, & Swati Kanchan. (2020). *Brain Tumor Classification (MRI)*[Data set]. Kaggle. https://doi.org/10.34740/KAGGLE/DSV/1183165

[15] Dale, B. M., Brown, M. A., & Semelka, R. C. (2015). *MRI: Basic Principles and Applications (Chapters 3 and 5)*. John Wiley & Sons.

[16] Kaur, R., GholamHosseini, H., Sinha, R., & Lindén, M. (2022). Melanoma Classification Using a Novel Deep Convolutional Neural Network with Dermoscopic Images. *Sensors, 22*(3), 1134. https://doi.org/10.3390/s22031134

[17] Johnson, J. M., & Khoshgoftaar, T. M. (2019). Survey on deep learning with class imbalance. *Journal of Big Data, 6(*1). https://doi.org/10.1186/s40537-019-0192-5

[18] Yasashvini, R., M, V. R. S., Panjanathan, R., S, G. J., & Anbarasi, L. J. (2022). Diabetic Retinopathy Classification Using CNN and Hybrid Deep Convolutional Neural Networks. *Symmetry, 14*(9), 1932. https://doi.org/10.3390/sym14091932

[19] Shaha, M., & Pawar, M. (2018). Transfer Learning for Image Classification. *2018 Second International Conference on Electronics, Communication and Aerospace Technology (ICECA)*. https://doi.org/10.1109/iceca.2018.8474802

[20] He, K., Zhang, X., Ren, S., & Sun, J. (2015). Deep Residual Learning for Image Recognition. *ArXiv (Cornell University)*. https://doi.org/10.48550/arxiv.1512.03385

[21] Simonyan, K., & Zisserman, A. (2015). Very Deep Convolutional Networks for Large-Scale Image Recognition. *International Conference on Learning Representations*. https://doi.org/10.48550/arXiv.1409.1556

[22] Tan, M., & Le, Q. V. (2019b). EfficientNet: Rethinking Model Scaling for Convolutional Neural Networks. *ArXiv (Cornell University)*. https://doi.org/10.48550/arXiv.1905.11946

[23] Ronneberger, O., Fischer, P., & Brox, T. (2015). U-Net: Convolutional Networks for Biomedical Image Segmentation. *ArXiv (Cornell University)*. https://doi.org/10.48550/arxiv.1505.04597

[24] Dosovitskiy, A., Beyer, L., Kolesnikov, A. I., Weissenborn, D., Zhai, X., Unterthiner, T., Dehghani, M., Minderer, M., Heigold, G., Gelly, S., Uszkoreit, J., & Houlsby, N. (2021). An Image is Worth 16x16 Words: Transformers for Image Recognition at Scale. *International Conference on Learning Representations*. https://doi.org/10.48550/arXiv.2010.11929

A Appendix

A.1 Data Certification.

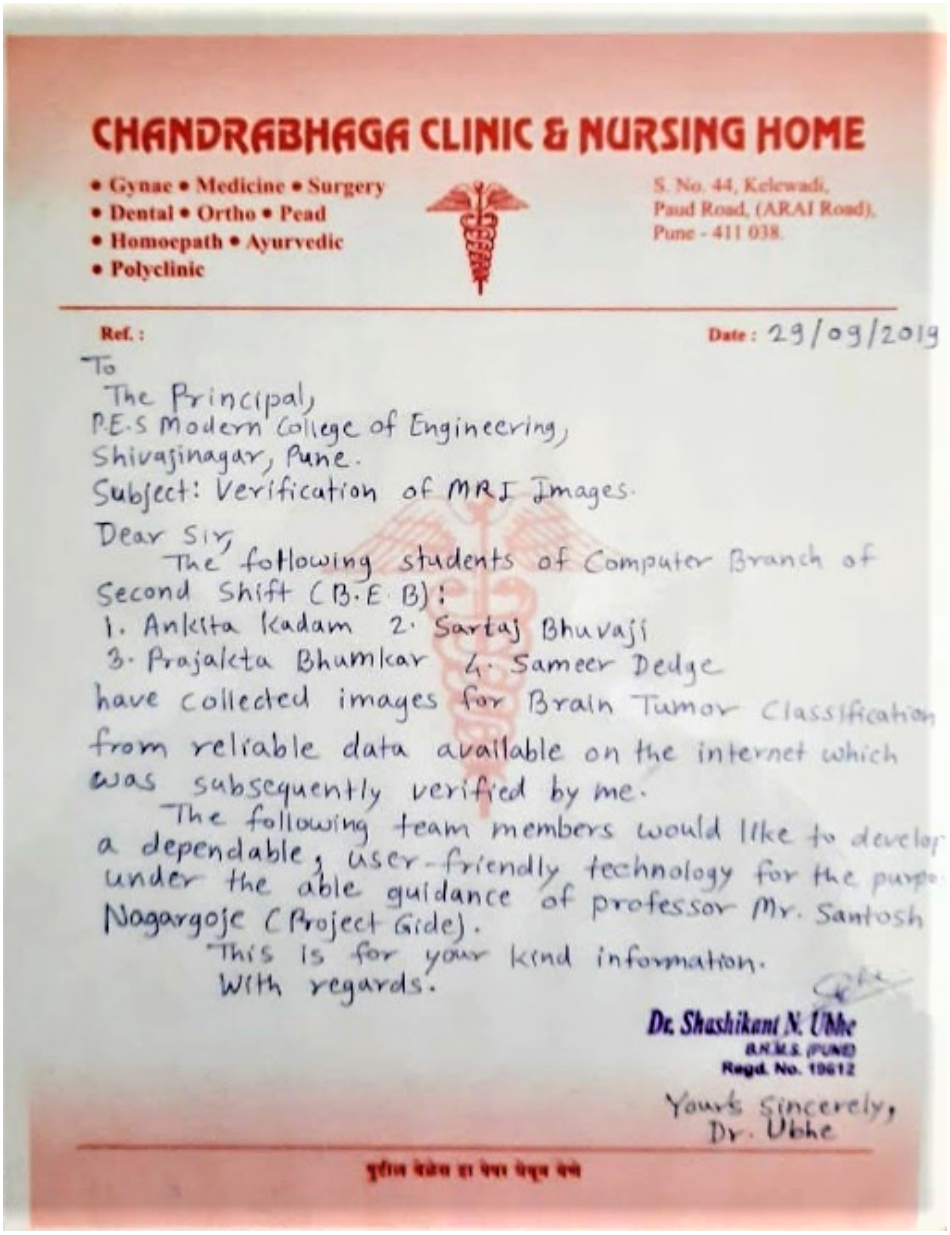

CHANDRABHAGA CLINIC & NURSING HOME

• Gynae • Medicine • Surgery
• Dental • Ortho • Pead
• Homoepath • Ayurvedic
• Polyclinic

S. No. 44, Kelewadi,
Paud Road, (ARAI Road),
Pune - 411 038.

Ref. : Date : 29/09/2019

To
The Principal,
P.E.S Modern College of Engineering,
Shivajinagar, Pune.
Subject: Verification of MRI Images.

Dear Sir,
The following students of Computer Branch of Second Shift (B.E. B):
1. Ankita Kadam 2. Sartaj Bhuvaji
3. Prajakta Bhumkar 4. Sameer Dedge
have collected images for Brain Tumor Classification from reliable data available on the internet which was subsequently verified by me.
The following team members would like to develop a dependable, user-friendly technology for the purpo under the able guidance of professor Mr. Santosh Nagargoje (Project Gide).
This is for your kind information.
With regards.

Dr. Shashikant N. Ubhe
B.H.M.S. (PUNE)
Regd. No. 19612

Yours Sincerely,
Dr. Ubhe

Fig. 4: The certification written by Dr. Shashikant Ubhe, which provides approval of the dataset [14].